JACS
JOURNAL OF THE AMERICAN CHEMICAL SOCIETY

Article

pubs.acs.org/JACS

Disentangling the Physical Processes Responsible for the Kinetic Complexity in Interfacial Electron Transfer of Excited Ru(II) Polypyridyl Dyes on TiO_2

David F. Zigler,* Zachary A. Morseth, Li Wang, Dennis L. Ashford, M. Kyle Brennaman, Erik M. Grumstrup, Erinn C. Brigham, Melissa K. Gish, Robert J. Dillon, Leila Alibabaei, Gerald J. Meyer, Thomas J. Meyer, and John M. Papanikolas*

Caudill, Kenan, and Murray Laboratories, Department of Chemistry, University of North Carolina at Chapel Hill, Campus Box 3290, Chapel Hill, North Carolina 27599, United States

Supporting Information

ABSTRACT: Interfacial electron transfer at titanium dioxide (TiO_2) is investigated for a series of surface bound ruthenium-polypyridyl dyes whose metal-to-ligand charge-transfer state (MLCT) energetics are tuned through chemical modification. The 12 complexes are of the form $Ru^{II}(bpy\text{-}A)(L)_2^{2+}$, where bpy-A is a bipyridine ligand functionalized with phosphonate groups for surface attachment to TiO_2. Functionalization of ancillary bipyridine ligands (L) enables the potential of the excited state $Ru^{III/*}$ couple, $E^{+/*}$, in 0.1 M perchloric acid ($HClO_4(aq)$) to be tuned from −0.69 to −1.03 V vs NHE. Each dye is excited by a 200 fs pulse of light in the visible region of the spectrum and probed with a time-delayed supercontiuum pulse (350−800 nm). Decay of the MLCT excited-state absorption at 376 nm is observed without loss of the ground-state bleach, which is a clear signature of electron injection and formation of the oxidized dye. The dye-dependent decays are biphasic with time constants in the 3−30 and 30−500 ps range. The slower injection rate constant for each dye is exponentially distributed relative to $E^{+/*}$. The correlation between the exponentially diminishing density of TiO_2 sub-band acceptor levels and injection rate is well described using Marcus−Gerischer theory, with the slower decay components being assigned to injection from the thermally equilibrated state and the faster components corresponding to injection from higher energy states within the ^{3}MLCT manifold. These results and detailed analyses incorporating molecular photophysics and semiconductor density of states measurements indicate that the multiexponential behavior that is often observed in interfacial injection studies is not due to sample heterogeneity. Rather, this work shows that the kinetic heterogeneity results from competition between excited-state relaxation and injection as the photoexcited dye relaxes through the ^{3}MLCT manifold to the thermally equilibrated state, underscoring the potential for a simple kinetic model to reproduce the complex kinetic behavior often observed at the interface of mesoporous metal oxide materials.

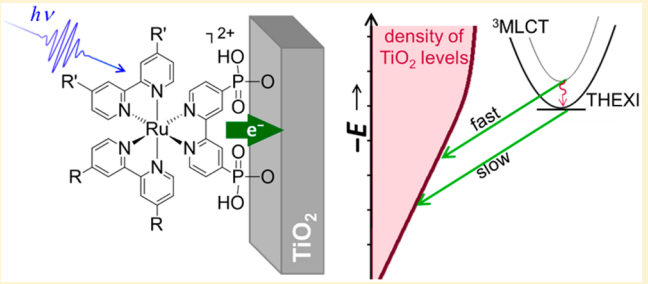

1. INTRODUCTION

Electron transfer from a photoexcited dye to a semiconductor provides a molecular basis for the conversion of light energy into potential energy in the form of an injected electron and an oxidized dye molecule. This reaction has been exploited for electrical power generation in dye-sensitized solar cells (DSSCs) and for chemical fuel production in dye-sensitized photoelectrochemical cells (DSPECs).[1−4] High conversion efficiencies require that this reaction, sometimes referred to as "photoinjection", "electron injection", or simply "injection", occurs quantitatively, behavior that is indeed observed at many dye−semiconductor interfaces. The central importance of the electron injection process has been widely recognized in many experimental studies, most notably with mesoporous nanocrystalline (anatase) TiO_2 thin films sensitized to visible light with organic and inorganic dyes.[5−7] Mechanistic studies performed with pulsed lasers have reported injection rates that range from the femto- to nanosecond time scales, behavior that is difficult to rationalize based on classical interfacial electron-transfer theories.[8−10] Until now, the underlying origin of this tremendous temporal range remains unknown, yet most speculation asserts that it results from heterogeneity in the mesoporous TiO_2 environment. Herein is reported an alternative interpretation that explains the kinetic heterogeneity in terms of a competition between excited-state relaxation and injection. A model is proposed based on a systematic kinetic study of 12 Ru(II) polypyridyl dyes that takes into account the exponential distribution of TiO_2 acceptor states[11−13] as the true origin of the remarkable range of injection rates available in the literature.

Received: December 12, 2015
Published: March 14, 2016

ACS Publications © 2016 American Chemical Society

DOI: 10.1021/jacs.5b12996
J. Am. Chem. Soc. 2016, 138, 4426−4438

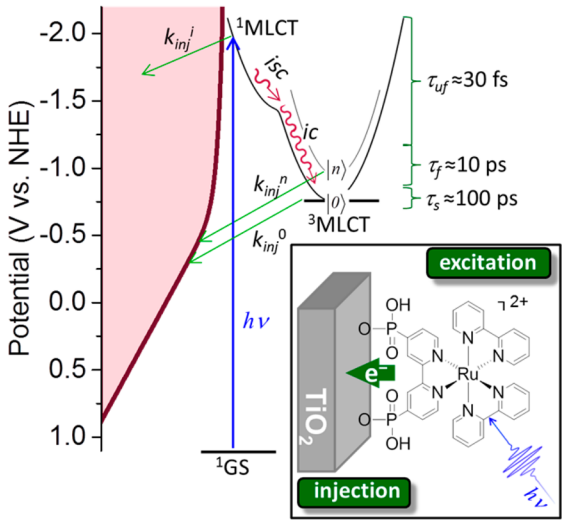

Figure 1. Inset is an illustration of a dye−semiconductor interface where the dye, bis(2,2′-bipyridine)(4,4′-bis(phosphono)-2,2′-bipyridine)-ruthenium(II) (**P**), is excited upon absorption of a photon $h\nu$ to either directly inject an electron into TiO_2 or to populate a singlet ^{1}MLCT that then relaxes or undergoes electron injection over a range of time scales, denoted τ_{uf}, τ_f, and τ_s. The semiquantitative energy diagram illustrates the mechanism of electron injection from lower ^{3}MLCT states for the dye **P** on TiO_2 into a continuum of acceptor levels in the semiconductor with an exponentially varying density of states. The ^{1}MLCT state undergoes electron injection into the TiO_2 on multiple time scales (k_{inj}^{x}), which also compete with relaxation through the excited-state manifold by intersystem crossing (isc) and internal conversion (ic) to the ^{3}MLCT state. The rate constants for injection on the picosecond time scale (k_{inj}^{n} and k_{inj}^{0}) correspond to injection from states ($|0\rangle$ and $|n\rangle$) in the lower portion of the ^{3}MLCT manifold.

A broad range of time scales is particularly evident in Ru(II) polypyridyl complexes. For this ubiquitous class of TiO_2 sensitizers, electron injection from the metal-to-ligand charge-transfer (MLCT) excited state extends from femtoseconds to picoseconds to nanoseconds (Figure 1). Early work showed that interfacial electron injection took place within femtoseconds after excitation.[8,14−17] Recent work from the Moran group[18] revealed that for a subset of the photoexcited ensemble, the Franck−Condon states are delocalized into the conduction band, and charge separation occurs simultaneously with excitation, as has been observed for a number of small organic systems including catachol and various perylene dyes.[19−22] This direct electron injection process is accompanied by a process involving electron transfer from the molecular excited state into the semiconductor, which has been observed by several groups to take place within 20−150 fs after excitation for a variety of Ru(II) dyes.[8,14,15,17,23] This fast time scale implies that injection from the initially populated ^{1}MLCT state competes with intersystem crossing, internal conversion, and interligand processes, all of which have been studied extensively in fluid solution for a number of Ru- (and Os-) polypyridyl complexes.[24−30] In addition to ultrafast injection, many groups report interfacial electron transfer occurring on the picosecond time scale.[8,14,16,31−36] These slower components account for a significant proportion (perhaps as much as 50%) of the injected electrons and exhibit complex kinetics that are poorly understood. They have been observed in a variety of systems and have been ascribed to a number of different microscopic phenomena, including variations in donor−acceptor coupling[37−39] or the density of semiconductor acceptor levels,[40,41] competition with vibrational cooling,[42] interligand electron transfer (ILET),[43] distal versus proximal injection,[43,44] semiconductor surface heterogeneity,[45,46] dye aggregation,[47−50] dye desorption, or dye binding mode,[37,51] whether physisorbed or chemisorbed.[23,52,53]

Because the electron injection process occurs in conjunction with excited-state relaxation (e.g., intersystem crossing, internal conversion, etc.) quantitative interpretations of experimental observation have proven elusive. A first complication stems from the difficulties associated with quantifying the injection kinetics. In many cases the kinetics are fit to stretched exponentials or to multiexponential functions from which an average injection time can be calculated; however, in aggregating the time constants, the microscopic dynamics of the dye/semiconductor interface are lost. A second complication arises from the difficulty in experimentally isolating specific system variables (e.g., driving force, electronic coupling, and reorganization energy). Changing pH, solvent, or ion concentration varies the density of conduction band levels (i.e., changes electron-transfer energetics),[11,54,55] but with concomitant changes to the local environment of the dyes.[56] Semiconductor materials with different conduction band edge positions provide a means to vary the energetic alignment between the dye and semiconductor acceptor levels and also modifies the electronic coupling of Ru(II) dye and the surface.[51,57−61] Attempts to unravel the excited-state dynamics using 3 or 4 Ru(II) dyes, between which the ruthenium-bound ligands were varied (e.g., CN^-, SCN^-, and bpy), were useful in revealing general trends,[8,33] but the significant differences in chemical structures necessitated the use of different reorganization energies for each complex, which made it difficult to interpret the injection rates solely within the context of Marcus−Gerischer theory. Without quantitatively accounting for changes in all relevant electron-transfer parameters, classical interfacial electron-transfer theory could not be directly applied, leaving room for speculation as to the physical phenomena underpinning the observed injection kinetics.

In this article we describe the interfacial electron-transfer dynamics in the time window spanning from 500 fs to 1.5 ns for 12 structurally similar Ru(II) polypyridyl dyes on TiO_2 in 0.1 M aqueous perchloric acid, $HClO_4$(aq). Surface binding for each complex utilizes a phosphonic acid derivatized 2,2′-bipyridine (bpy), with or without a $-CH_2-$ spacer. Under these conditions, the surface linkage is by phosphonate group esters, e.g., (Ti-OP(O)OH)$_2$bpy.[32] Two additional bpy ligands with varying substituents in the 4,4′ positions are used to systematically tune reduction potentials of the excited-state couple ($Ru^{III/*}$), Figure 2, and thus the driving force while preserving the $Ru(bpy)_3^{2+}$-like core. The 12 dyes are divided into two series with different electronic couplings for electron transfer. In the **P**-series, the phosphonic acid groups are directly attached to the bipyridine ligand, in contrast to the homologous **CP**-series where a methylene spacer is inserted between the bipyridine ligand and phosphonic acid anchor. Femtosecond transient absorption spectroscopy reveals two kinetic components in the electron injection dynamics (Figure 1). The slower component (30−500 ps) we interpret as corresponding to injection from the thermally equilibrated excited state, i.e. the so-called THEXI state, while the fast component is consistent with injection from higher energy states within the ^{3}MLCT manifold. Furthermore, the two injection components are kinetically coupled and can be described by a single kinetic model, which is in stark contrast

DOI: 10.1021/jacs.5b12996
J. Am. Chem. Soc. 2016, 138, 4426−4438

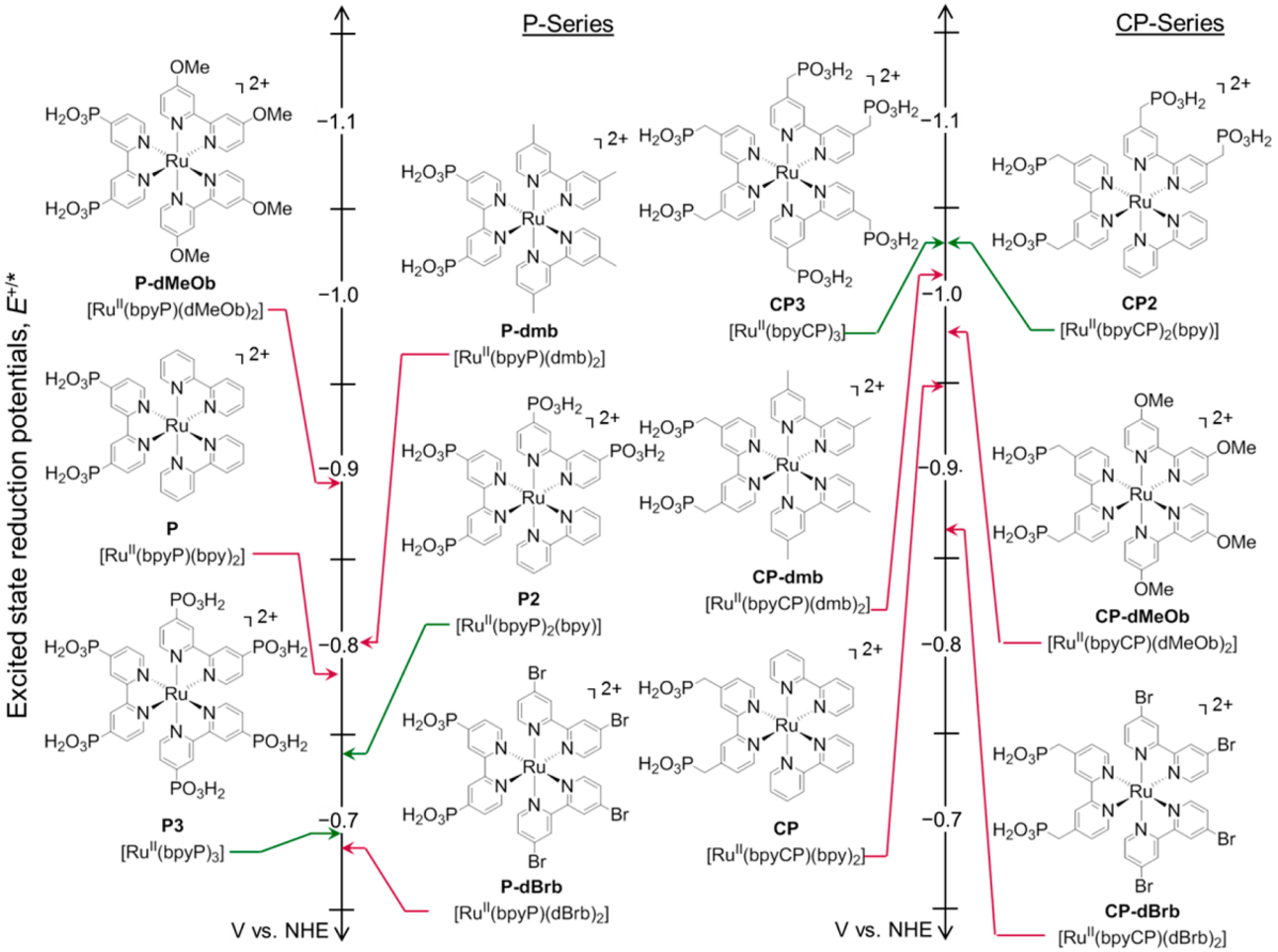

Figure 2. Ru(II) polypyridyl dyes studied on TiO_2 showing relative potentials ($E^{+/*}$) for the excited-state reduction, $Ru^{III/*}$. Dyes with one ligand capable of surface binding to TiO_2 (subseries **P-dRb** and **CP-dRb**) are indicated by use of red arrows, and dyes with multiple anchoring groups are indicated with green (subseries **P*x*** and **CP*x***).

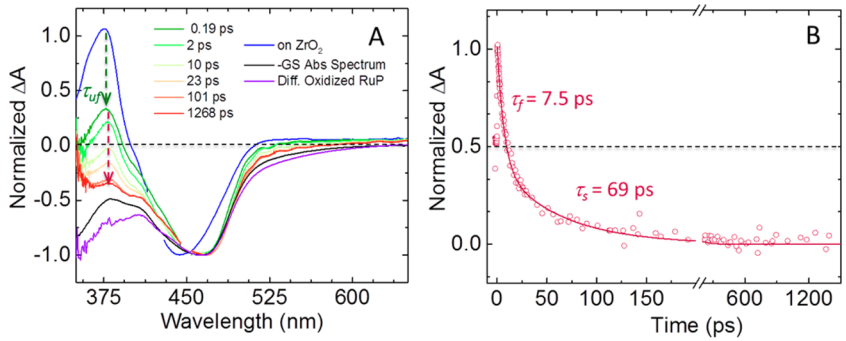

Figure 3. (A) Transient absorption spectrum obtained following the excitation of **P** on ZrO_2 (blue) and TiO_2 (green to red). Also shown are the inverse of the ground-state absorption spectrum (black) and difference spectrum, $\Delta A = A(\mathbf{P}^+) - A(\mathbf{P})$, obtained by electrochemical oxidation of **P** on the TiO_2 surface (violet). (B) Normalized decay at 376 nm (points) along with fit to a biexponential function (solid line). All spectra were measured in argon purged 0.1 M $HClO_4$(aq) when excited with a 200 fs, 100 nJ pulse exciting into the MLCT band and with a 120 μm diameter spot size.

to current conventional descriptions that invoke interfacial heterogeneity to explain the multiexponential behavior.

2. RESULTS AND DISCUSSION

This work brings together multiple experimental and theoretical techniques to build a mechanistic model for the excited-state interfacial electron-transfer dynamics of Ru(II) polypyridyl complexes bound to nanocrystalline TiO_2. Broadband ultrafast transient absorption spectroscopy is used to characterize the multiple time scales for injection (Section 2.1). We discuss the interfacial electron injection in the context of Marcus−Gerischer theory (Section 2.2), which motivates the characterization of the excited dye energetics and TiO_2 acceptor levels. Electrochemical measurements of the reduction potential at the $Ru^{III/II}$ couple are used in conjunction with emission spectral fitting to determine the standard reduction potentials of the MLCT excited state, $E^{+/*}$, while spectroelectrochemistry is used to measure the

DOI: 10.1021/jacs.5b12996
J. Am. Chem. Soc. 2016, 138, 4426−4438

density of acceptor states in the nanocrystalline-TiO_2 films (Section 2.3). The experimentally determined energetic and kinetic data are examined in the context of Marcus−Gerischer theory, leading to a simplified mechanistic model for electron injection (Section 2.4).

2.1. Spectroscopic Signature of Electron Injection. The rates of electron injection are measured by broadband transient absorption spectroscopy following photoexcitation to the ^{1}MLCT state by a femtosecond laser pulse. A representative series of transient absorption spectra obtained from **P** are depicted in Figure 3. These spectra exhibit all of the characteristic features that are generally found in the transient spectra of Ru(II) polypyridyl complexes. The negative going feature near 450 nm corresponds to a bleach of the ground-state ^{1}MLCT absorption band, while the excited-state absorption centered near 376 nm arises from a $\pi \rightarrow \pi^*$ transition of the bpy$^{\bullet-}$ radical anion. In addition to these prominent features, there is a weak absorption band that extends to the red of 500 nm that has been assigned to bpy$^{\bullet-}$ radical $\pi \rightarrow \pi^*$ transitions[62] and ligand-to-metal charge-transfer (LMCT) bands of the excited state.[14]

In fluid solution, the intensity of the bpy$^{\bullet-}(\pi \rightarrow \pi^*)$ absorption is typically comparable to the magnitude of the bleach. This is also the case on ZrO_2, which has surface properties similar to TiO_2 but is inert toward injection because the conduction band is energetically inaccessible (Figure 3). The same dye on TiO_2 shows similar features, but as time increases there is a distinct decrease in the intensity of the bpy$^{\bullet-}(\pi \rightarrow \pi^*)$ band relative to the bleach. The spectrum at 1200 ps resembles the inverse of the ground-state absorption spectrum of **P** in solution (black) and is also similar to the difference spectrum obtained following electrochemical oxidation to Ru(III) (violet). The loss of the excited-state bpy$^{\bullet-}(\pi \rightarrow \pi^*)$ absorption band without the decay of the MLCT bleach intensity is consistent with the formation of the oxidized dye and provides a direct signature of electron injection. The physical origin of the spectral shift in the bleach between TiO_2 and ZrO_2 is not entirely clear. Similar variation in the positions and/or widths of the bleach features on TiO_2 and ZrO_2 is observed to differing degrees, for all of the complexes. We do note that these differences are generally smaller in the **CP**-series complexes (Figure S1), where the phosphonate linkers are separated from the π-network of the ligand by a methylene spacer, suggesting that they could stem from different interactions with the two semiconductor substrates.

The intensity of the bpy$^{\bullet-}(\pi \rightarrow \pi^*)$ absorption at the earliest delays (~200 fs) on TiO_2 is only about half that observed on ZrO_2, suggesting that ~50% of the injection events occur within our instrument response time.[63] The remaining intensity decays over 400−500 ps and fits well to a biexponential function (Figure 3B) with a fast time constant near 7.5 ps and a slower time constant near 69 ps. The rate of recombination can depend upon excitation intensity[64] which likely influences subsequent injection kinetics. However, all of the experiments discussed here employed sample translation and were performed at pulse energies <~100 nJ (120 μm spot size), where it was confirmed that the recombination kinetics were independent of pump intensity.

As with **P**, all of the Ru(II) dyes depicted in Figure 2 exhibit the same signatures of electron injection but with significant variations in time scale. Figure 4 shows the decays of the bpy$^{\bullet-}(\pi \rightarrow \pi^*)$ absorption at 376 nm for all 12 dyes. For purposes of comparison, each decay is normalized between the signal observed at the earliest (~200 fs) and longest (1.5 ns) time delays, i.e.

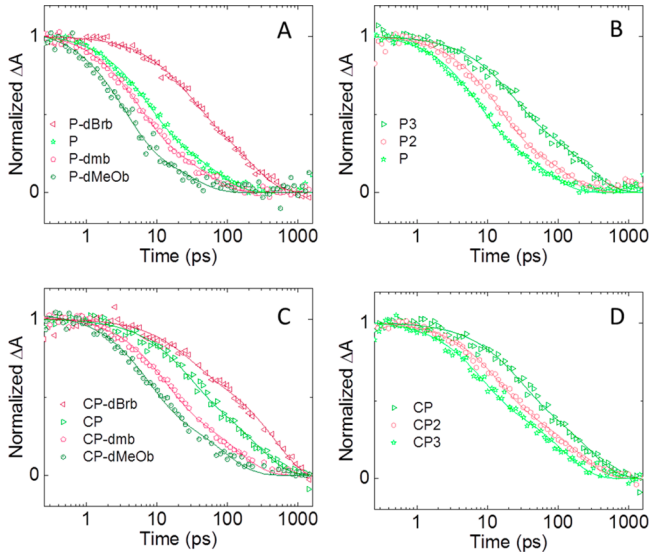

Figure 4. Decay of the bpy$^{\bullet-}(\pi \rightarrow \pi^*)$ absorption monitored at 376 nm (points) for the 12 different dyes examined in this study. Also shown are fits of the decays to biexponential decay functions (lines). The transient data were also fit to a Kohlrausch−Williams−Watts function (Figure S2 and Table S1), but since the stretched exponential does not have an underlying physical basis, it was not pursued in the analysis. Samples were continuously translated to minimize cumulative damage to the sample. Absorption spectra acquired after the experiment were identical to initially collect spectra. The pump energy was 80−100 nJ per pulse with a 120 μm spot, and the excitation wavelength was varied from 420 to 535 nm with no obvious change in the kinetics in the time window studied. Each decay represents the average observed for a minimum of 6 different TiO_2 slides and 6000−12000 averaged measurements per time-point per slide.

$$\Delta\tilde{A}_t^R = \frac{\Delta A(t) - \Delta A(\infty)}{\Delta A(0) - \Delta A(\infty)} \quad (1)$$

The transients show that the injection process occurs with multiple time scales, generally represented as

$$\Delta\tilde{A}_t^R = A_{uf}e^{-(\tau_{uf}^{-1}t)} + A_f e^{-(\tau_f^{-1}t)} + A_s e^{-(\tau_s^{-1}t)} \quad (2)$$

with all but complex **CP-dBrb** appearing to decay completely by 1 ns. The instrument response of our spectrometer is not sufficient to capture the very early time events that have been reported by a number of groups,[32,65−68] which corresponds to the "ultrafast" component (i.e τ_{uf}) in eq 2. Since our focus is on the picosecond dynamics, we have normalized the injecting population to the sum of the fast and slow components. Although our analysis does not consider the "ultrafast" component, these sub-200 fs injection events can be placed within the context of the physical model that is developed, as is discussed near the end of Section 2.4.

The fast (τ_f) and slow (τ_s) decay components, along with amplitudes (A_f, A_s) are summarized for the 12 complexes in Table 1. The injection rate increases with increasing electron-donating ability of the substituents on the dye (e.g., **P-dMeOb** > **P-dBrb**) and when the phosphonate linkage is bound directly to bipyridine (e.g., **P** > **CP**). The physical origin of these effects is discussed in more detail in Section 2.4.

2.2. Marcus−Gerischer Theory of Interfacial Electron Transfer. In developing a framework to describe the observed

DOI: 10.1021/jacs.5b12996
J. Am. Chem. Soc. 2016, 138, 4426−4438

Table 1. Time Constants and Amplitudes from Biexponential Fits to the Decays Probed at 376 nm in 0.1 M $HClO_4$(aq)[a]

dye	τ_f (ps)	A_f[b]	τ_s (ps)	A_s[b]
		P-dRb Series		
P-dMeOb	3.6(±0.2)	0.75(±0.05)	32(±8)	0.25(±0.05)
P-dmb	5.3(±0.4)	0.65(±0.03)	53(±6)	0.35(±0.03)
P	7.5(±0.5)	0.62(±0.02)	69(±0.6)	0.38(±0.02)
P-dBrb	26(±3)	0.45(±0.04)	200(±16)	0.55(±0.04)
		CP-dRb Series		
CP-dMeOb	7.1(±0.6)	0.59(±0.03)	86(±8)	0.41(±0.03)
CP-dmb	11(±1)	0.53(±0.02)	126(±6)	0.47(±0.02)
CP	30(±3)	0.50(±0.03)	303(±23)	0.50(±0.03)
CP-dBrb	28(±3)	0.32(±0.02)	471(±25)	0.68(±0.02)
		P*x* Series		
P	7.5(±0.5)	0.62(±0.02)	69(±0.6)	0.38(±0.02)
P2	12(±2)	0.59(±0.04)	110(±14)	0.41(±0.05)
P3	19(±2)	0.48(±0.03)	218(±17)	0.52(±0.03)
		CP*x* Series		
CP	30(±3)	0.50(±0.03)	303(±23)	0.50(±0.03)
CP2	13(±1)	0.51(±0.02)	179(±8)	0.49(±0.02)
CP3	7.2(±0.7)	0.49(±0.02)	117(±8)	0.51(±0.02)

[a]At room temperature. Errors are from the nonlinear least-squares fit to the bin-averaged decay traces. [b]Amplitudes are normalized to the sum of A_{vf} and A_f.

injection rates, we turned to the semiclassical expression of Marcus−Gerischer theory. As derived by Marcus[69] and Hush[70] and applied to interfacial semiconductor electron transfer by Gerischer in the classical limit,[71] the rate constant for electron transfer depends on the driving force (ΔG^{o}_{ET}), the reorganization energy for the excited dye $Ru^{III/*}$ couple (λ), and electronic coupling matrix element (H_{AB}) between the excited state and oxide surface for a single level in the oxide, i.e.

$$k^{0}_{ET}(E, E^{+/*}) = \frac{2\pi}{\hbar}|H_{AB}|^2 \frac{1}{\sqrt{4\pi\lambda k_B T}} \exp\left(\frac{-(\lambda + \Delta G^{o}_{ET}(E, E^{+/*}))^2}{4\lambda k_B T}\right) \quad (3)$$

The driving force can be expressed in terms of electrochemical potentials as

$$\Delta G^{o}_{ET}(E, E^{+/*}) = -F(E, E^{+/*}) \quad (4)$$

where $E^{+/*}$ is shorthand notation for the standard reduction potential of the photoexcited dye (i.e., $E^{\circ}(Ru^{III/*})$), E is electrode potential of the acceptor level in the semiconductor, and F is the Faraday constant (1 eV/V). The rate is maximized to acceptor levels where ΔG^{o}_{ET} is equal to the negative of the reorganization energy (i.e., $E = E^{+/*} + \lambda/F$).[71] The classical electron-transfer barrier increases for larger or smaller driving forces, which in addition to resulting in slower electron-transfer rates corresponds to the inverted and normal Marcus regimes, respectively (Figure 5).

The rate constant for injection into a semiconductor is not the rate constant associated with a single acceptor level but rather reflects injection into a quasi-continuous distribution of levels that consist of delocalized conduction band states and localized trap states. The distribution of electron-transfer rates is weighted by this density of acceptor states, as illustrated in Figure 5, is small near the band edge, and increases at higher energy (i.e., more negative potentials). As a result, an activationless rate is predicted for acceptor levels with E slightly more negative than $E^{+/*}+\lambda/F$.

The injection rate is obtained from eq 3 by integrating over all the acceptor level potentials to obtain the final Marcus−Gerischer expression, i.e.

$$k^{0}_{inj}(E^{+/*}) = -\frac{2\pi}{\hbar}|H_{AB}|^2 \frac{1}{\sqrt{4\pi\lambda k_B T}} \times \int_{E_{\emptyset}}^{E_{vac}} \rho_0(E) \times \exp\left(\frac{-(\lambda + \Delta G(E, E^{+/*}))^2}{4\lambda k_B T}\right) dE \quad (5)$$

where $\rho_0(E)$ is the number of acceptor levels between E and $E + dE$; $E_{\emptyset}$ is a potential where the density of acceptor levels is zero positive of (below) the TiO_2 conduction band edge (E_{CB}), and E_{vac} is the vacuum potential.[72] The application of eq 5 to analyze the transient kinetic data requires an independent measure of dye energetics (i.e., $E^{+/*}$) as well as the semiconductor density of states ($\rho_0(E)$). Experimental determination of both is described in Section 2.3.

2.3. System Energetics. *2.3.1. Excited-State Energetics.* The MLCT excited-state energy landscape for the Ru(II) polypyridyl complexes is best described in terms of three separate energy wells that correspond to the electron being localized on one of the three bpy ligands. In homoleptic complexes the three ligands have the same energy in the isolated complex, while in solution the solvent environment lifts the degeneracy within the ligand set, accounting for an approximately 2500 cm^{-1} energy

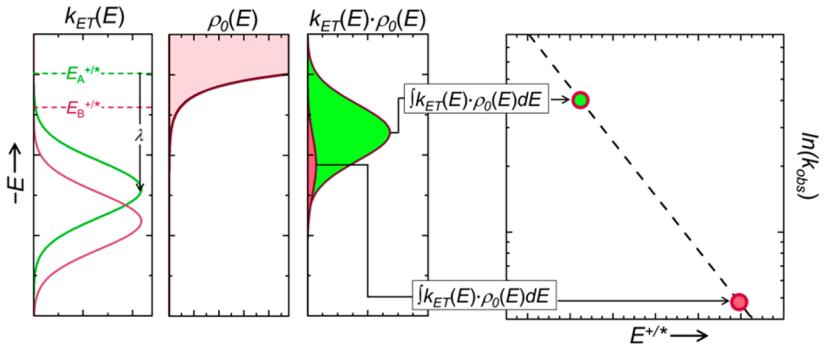

Figure 5. For dyes of different donor strength ($E_A^{+/*}$, $E_B^{+/*}$) injecting into a band gives a distribution of second-order injection constants, $k_{ET}(E)$. A maximum rate occurs for injection into levels for which the free energy difference from the excited state is equal to the solvent reorganization, i.e., $E = E^{+/*} + \lambda/F$. For structurally similar dyes/semiconductor systems, the maximum is offset by the difference in excited-state reduction potential. The distribution of acceptor levels is described by the density of states function, $\rho_0(E)$. The product $k_{ET}(E)\cdot\rho_0(E)$ is proportionally higher for excited states which sample a higher density of states. The integrated product results in an injection rate constant, k_{obs}, dependent on $E^{+/*}$, e.g., $k_{obs}(E_A^{+/*}) > k_{obs}(E_B^{+/*})$. The distribution of rate constants k_{obs} with respect to $E^{+/*}$ mirrors $\rho_0(E)$, with k_{obs} shown exponentially distributed for an exponential $\rho_0(E)$.

DOI: 10.1021/jacs.5b12996
J. Am. Chem. Soc. 2016, 138, 4426−4438

difference between highest and lowest solvent stabilized MLCT states (as calculated for $Os(bpy)_3^{2+}$).[25] For Ru(II) dyes (e.g., $Ru(bpy)_3^{2+}$), the excitation localized on one ligand and one $Ru(d\pi^5)$ hole undergoes an interligand electron/inter-$Ru(d\pi^5)$ hole-transfer process that moves the excited-state dipole around the dye (more simply referred to as ILET).[66,73] Ligand substituents attached to one (or two) of the three ligands also lift the degeneracy of the three lowest MLCT states, with electron-withdrawing substituents lowering the energy of MLCT states associated with that bpy ligand. Thus, the thermally equilibrated MLCT state distribution in heteroleptic complexes is directed toward the more electron deficient ligand(s).[74] With energetically inequivalent ligands the forward and reverse ILET rate constants are modified by the driving force.[24] The consequence of ILET for TiO_2 bound MLCT states is that portions of the excited population may have electron density localized away from the interface, and in these systems the injection process would be convoluted with ILET dynamics taking place within the MLCT manifold. This presents a kinetic picture with two limits. In the first limit, ILET is fast relative to injection resulting in injection that is only dependent on ΔG^{o}_{ET}. In the second limit ILET is much slower, resulting in injection from the thermalized population of MLCT states, thus giving kinetic components reflective of proximal and distal injection and for which the relative contribution of each would be independent of the observed rate. Thus, there are two central questions that must be addressed with regard to the MCLT excited-state (or states) energies: (i) What is the energy of the lowest-lying MLCT state in relation to the TiO_2 conduction band energy levels and density of states? and (ii) on which ligand(s) does the lowest energy MLCT state reside?

To address the first question we have combined electrochemical and steady-state photoluminescence (PL) measurements to determine excited-state energies for the series of Ru(II) dyes. Excited-state reduction potentials ($E^{+/*}$, Table 2) are determined from the $E°(Ru^{III/II})$ reduction potential and the free energy change between the ground state and excited state (ΔG^{o}_{ES}), i.e.

$$E^{+/*} = E°(Ru^{III/II}) - \Delta G^{o}_{ES}/F \quad (6)$$

with

$$\Delta G^{o}_{ES} = \mathbf{E}_0 + \lambda_{ES} \quad (7)$$

where $\mathbf{E}_0$ is the energy gap obtained from a fit to the PL spectrum using a single-mode approximation, and λ_{ES} is the classical reorganization energy between excited and ground states with contributions from all of the vibrational modes.[75−78] All three quantities ($E°(Ru^{III/II})$, $\mathbf{E}_0$, λ_{ES}) are determined experimentally for each dye (Table 2). Ground-state reduction potentials, $E°(Ru^{III/II})$, are measured on TiO_2 in 0.1 M $HClO_4$(aq). Both $\mathbf{E}_0$ and λ_{ES} are determined from an emission spectral fitting analysis of the PL spectra measured on ZrO_2 (Supporting Information).[76,77,79]

A comparison of the electrochemical and photophysical data shows that substituents on the ancillary ligands affect the lowest excited state in two ways. The addition of electron-donating substituents increases the electron density at the metal center, causing the $E°(Ru^{III/II})$ potential to shift to more negative, consistent with Lever.[80] This shift in the ground-state potentials is also observed for the excited state ($E^{+/*}$). However, because there is a systematic decrease in the free-energy of the excited state relative to the ground state (ΔG^{o}_{ES}) that also correlates with

Table 2. Ground- and Excited-State Reduction Potentials ($E°(Ru^{III/II})$, $E^{+/*}$) for the Series of Chromophores on TiO_2 in 0.1M $HClO_4$(aq), All versus NHE[a]

	TiO_2	ZrO_2			
dye	$E°(Ru^{III/II})$ (V)[b]	$\mathbf{E}_0$ (eV)[c]	λ_{ES} (eV)[c]	ΔG^{o}_{ES} (eV)[c]	$E^{+/*}$ (V)[d]
P-dRb Series					
P-dMeOb	1.08	1.76	0.19	1.96	−0.89
P-dmb	1.19	1.86	0.14	1.99	−0.80
P	1.28	1.90	0.15	2.06	−0.78
P-dBrb	1.45	1.96	0.17	2.13	−0.68
CP-dRb Series					
CP-dMeOb	1.07	1.90	0.15	2.05	−0.98
CP-dmb	1.12	1.96	0.17	2.13	−1.01
CP	1.22	2.01	0.16	2.17	−0.95
CP-dBrb	1.16	1.87	0.16	2.03	−0.87
P*x* Series					
P	1.28	1.90	0.15	2.06	−0.78
P2	1.33	1.91	0.16	2.07	−0.74
P3	1.43	1.94	0.17	2.12	−0.69
CP*x* Series					
CP	1.22	2.01	0.16	2.17	−0.95
CP2	1.13	1.99	0.17	2.16	−1.03
CP3	1.12	1.98	0.17	2.15	−1.03

[a]Results of electrochemical measurements performed in solution at a glassy carbon electrode are given in Table S1. [b]The potential was measured against Ag/AgCl which was calibrated against SCE (0.241 V vs NHE) and the III/II couple of $[Ru(bpy)_3]^{2+}$ (1.26 V vs NHE). [c]$\Delta G^{o}_{ES} = \mathbf{E}_0 + \lambda_{ES}$. [d]$E^{+/*} = E°(Ru^{III/II}) - \Delta G^{o}_{ES}/F$.

electron-donating ability, the overall shift observed in $E^{+/*}$ is smaller than that observed in $E°(Ru^{III/II})$.

To address the second question we turned to density functional theory (DFT) to provide insight into the ligand energy alignment. As shown in Figures 6 and S5, the highest occupied molecular orbitals (HOMO−2, HOMO−1, and HOMO) are localized on the Ru(II) center, and the unoccupied orbitals (LUMO, LUMO+1, LUMO+2) are situated on the bpy ligands. One of the three LUMO orbitals is localized on the bpyP (or bpyCP) anchoring ligand. Because the calculations represent the solvent as a dielectric continuum, the two ancillary ligands are nearly degenerate, and as a result the other two LUMO orbitals have amplitude on both ligands. This delocalization is a consequence of molecular symmetry in the calculation and is not present in the experimental system since the molecular nature of the solvent makes the energies of all three ligands distinct, as has been noted in time-dependent anisotropy studies of similar dyes.[24] Nevertheless, when considering the unoccupied orbitals (LUMO, LUMO+1, and LUMO+2), a general theme emerges that electron-donating groups destabilize both the HOMO and LUMO (Figure 6), consistent with the electrochemical measurements. For the **P-dRb** series the LUMO is localized largely on the bpyP ligand, suggesting that for this set of dyes the lowest energy MLCT excited state is located on the ligand bound to the surface. While the LUMO has no amplitude on the ancillary ligands for the **P**, **P-dmb**, and **P-dMeOb** complexes, in **P-dBrb** a small amount of electron density is observed on the dBrb ligand, consistent with a smaller energy gap between the MLCT states localized on the different ligands (see Supporting Information). In the case of the **CP-dRb** series, the phosphonic acid with the methylene spacer destabilizes the bpyCP ligand relative to the distal ligands. The replacement of an

DOI: 10.1021/jacs.5b12996
J. Am. Chem. Soc. 2016, 138, 4426−4438

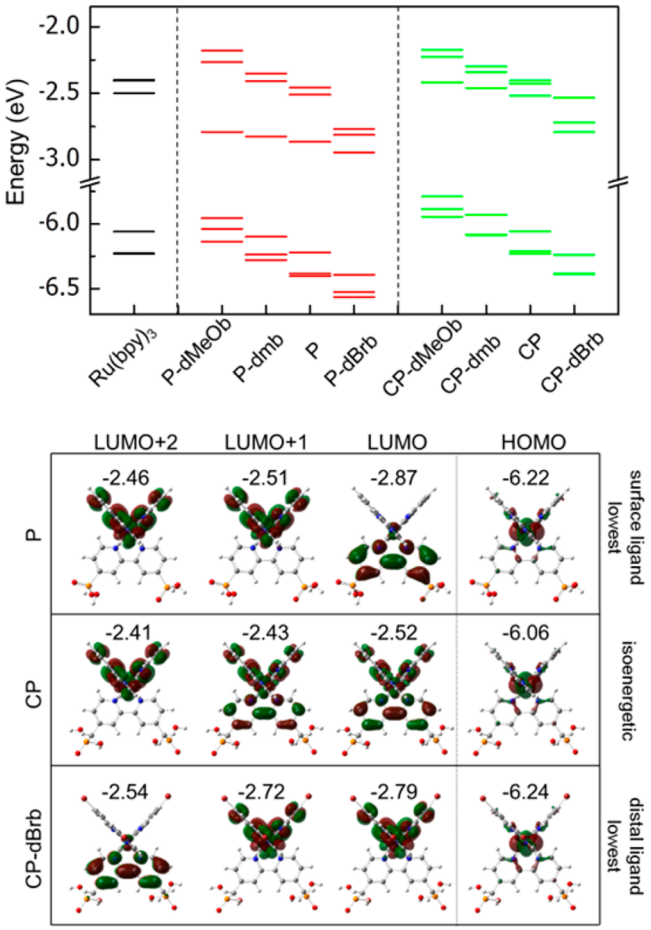

Figure 6. (Top) Frontier orbital energies (HOMO−2, HOMO−1, HOMO, LUMO, LUMO+1, and LUMO+2) obtained from DFT calculations for the representative set of chromophores studied here. Calculations were performed using the B3LYP functional with mixed basis for the ruthenium atom (LANL2DZ) and all other atoms (6-31G**). (Bottom) HOMO and LUMO obtained from DFT) calculations in a polarizable continuum medium (PCM) for **P**, **CP**, and **CP-dBrb** (isovalue = 0.03) illustrating the changes to LUMO localization effects attributable to ligand substituents.

electron-withdrawing phosphonate substituents on the bpyP ligand by electron-donating methylenephosphonate increases the π^*-orbital energy, but the phosphonate ligand is still predicted to be lowest in energy for the **CP-dMeOb** and **CP-dmb** complexes. For the **CP** complex, the DFT results suggest that the three ligands should be nearly isoenergetic, and for **CP-dBrb**, the π^*-levels of the ancillary ligands are predicted to be lowest lying.

Experimental support of the ligand energy predictions from DFT comes from the dyes' PL spectra (Figure S4). In solution, the room-temperature PL spectrum includes contributions from the thermally equilibrated population distributed among all three MLCT states. For the **P-dRb** series, the PL emission maximum in solution systematically red shifts with increasing electron-donating ability of the substituents, from 636 nm (**P-dBrb**) to 723 nm (**P-dMeOb**). This systematic red shift results from a combination of factors. The electron-donating substituents destabilize the Ru(dπ) orbital as well as the π^* orbitals of all three ligands. The magnitude of the destabilization however is not the same, with the ancillary ligands being destabilized the most and the π^* levels of the phosphonated ligands destabilized the least. The red shift in the PL with increasing electron-donating ability is consistent with the destabilization of the Ru(dπ) orbital being greater than that of the emitting orbital, suggesting that the PL is originating from the MLCT state associated with the bpyP ligand. As with the complexes in the **P-dRb** series, the **CP**, **CP-dmb**, and **CP-dMeOb** complexes also show a systematic red shift in their PL, consistent with the phosphonate ligand being lowest in energy. The PL of **CP-dBrb** (661 nm), however, is lower in energy compared to **CP** (627 nm), suggesting that the lowest MLCT state in that complex is localized on the ancillary ligand.

The changes observed in the PL spectra upon attachment to ZrO_2 provide further corroboration of the DFT predictions. The PL spectra from the complexes with electron-donating substituents on the distal ligands (e.g., **P-dMeOb**, **P-dmb**, **P**, **CP-dMeOb**, **CP-dmb**) show a distinct blue shift upon surface attachment. For example, the PL spectrum of **P-dMeOb** blue shifts 400 cm^{-1} upon attachment to ZrO_2. This spectral shift could be evidence that for these complexes the MLCT excited state is localized on the phosphonate ligand. Others suggested that dyes form tightly packed monolayers on the metal-oxide surface, although this suggestion is difficult to confirm experimentally due to the uncertainty in determining the "true" area of the oxide.[12] A tightly packed binding mode significantly changes the local environment of the ligand closest to the interface, while having less of an effect on the portion exposed to solvent. Restricted access to the solvent would destabilize the bpyP and bpyCP ligands relative to the ancillary ligands, resulting in the spectral blue shift. When the phosphonate ligand is highest in energy, or isoenergetic with the other ligands, the PL will also have a contribution from MLCT states localized on the distal ligands. As a result, the emission spectra for those complexes should be unaffected by surface attachment, which appears to be the case for the complexes predicted by DFT to have nearly isoenergetic ligands (e.g., **P3**, **P-dBrb**, **CP**).

In summary, based on these observations, the thermally equilibrated MLCT state population has electron density localized near the surface for Ru(II) dyes in which the ancillary ligands are more electron rich than the anchoring ligand, including **P-dMeOb**, **P-dmb**, **P**, **CP-dMeOb**, and **CP-dmb**. The complexes **P-dBrb**, **P2**, **P3**, **CP**, **CP2**, and **CP3** have nearly isoenergetic anchoring and ancillary ligands, likely resulting in a nearly isotropic distribution of MLCT states. The LUMO for **CP-dBrb** appears to be localized on the ancillary ligands, probably resulting in the thermally equilibrated MLCT population localized away from the surface.

2.3.2. Measured Density of States. In the Marcus−Gerischer representation, the dependence of the injection rate on excited-state reduction potential, $E^{+/*}$, is dictated by the functional form of the density of states, $\rho_0(E)$. One common approach assumes a parabolic band description for the semiconductor, where $\rho_0(E) \propto \sqrt{E}$.[11,54] For nanocrystalline films this description is an inadequate representation of states near or below the conduction band edge. Debate continues over the distribution and nature of conduction bands levels in nanocrystalline TiO_2 films.[12,13,81] Several functional forms of $\rho_0(E)$ for TiO_2 have been put forth that were either empirically derived or determined from calculation.[13,54,65,82] The density of levels near the conduction band for TiO_2 can depend sensitively on the preparation of the film, making it inappropriate to use these forms directly.

We have used spectroelectrochemistry to directly determine the density of states for the same sensitized TiO_2 films used in the ultrafast experiments (Figure S7).[54,83,84] Because the TiO_2

DOI: 10.1021/jacs.5b12996
J. Am. Chem. Soc. 2016, 138, 4426−4438

conduction band levels are sensitive to the pH and ionic strength, these measurements were also carried out under identical experimental conditions, i.e., 0.1 M $HClO_4$(aq). This measurement yields the integrated density of acceptor (i.e., unfilled at open circuit) levels positive of the applied potential (E_a). The details regarding the measurement are described in the Supporting Information, and the results are depicted by the individual points in Figure 7.

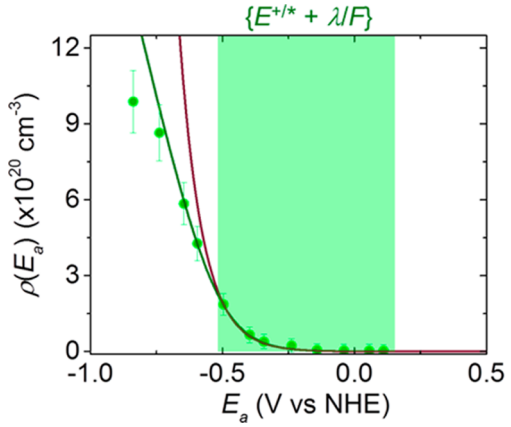

Figure 7. Spectroelectrochemically determined[54,89] integrated density of states function, $\rho(E_a)$, (green circles) of a TiO_2 film derivatized with **CP-dmb** in 0.1 M $HClO_4$. The error bars result from the detection limit of the spectrophotometer used and from error propagated by measurements of film thickness (4.6 ± 0.3 μm) and estimation of film density (0.4 ± 0.02 v/v film). The lines represent nonlinear least-squares fits to the data, using either a bulk band with traps model (green) or exponential distribution of sub-band states (red). The green shaded region shows the potential range that is relevant for the series of excited Ru(II) polypyridyl dyes.

The relationship between the integrated density of states function $\rho(E_a)$ and the distribution of acceptor levels $\rho_0(E)$ is

$$\rho(E_a) = -\int_{E_\emptyset}^{E_a} \rho_0(E)dE \tag{8}$$

where $E_\emptyset$ corresponds to an applied potential below the conduction band edge (E_{CB}), and the density of acceptor level is zero. At the conduction band edge (E_{CB}), an exponential distribution of states is observed, and this distribution for nanocrystalline TiO_2 is far broader than that predicted by simple thermal broadening of the bulk band-edge.[12,13,82] Bisquert and co-workers[85] have characterized the nonideality (α) of the exponential tail for films of different size TiO_2 particles as

$$\rho_0(E) = \frac{\alpha F V_m N_x}{k_B T} \exp\left(\frac{\alpha F}{k_B T}(E_{CB} - E)\right) \tag{9}$$

where N_x is the total number of acceptor levels per cm^3 that lie between $E_\emptyset$ and E_{CB}, which is taken to be −0.22 V vs NHE in pH 1.[11] The volume normalization term (V_m) is calculated from the unit cell volume (V_0) and an estimate of the number of unit cells that the excited dye can access (N_m), i.e., $V_m = V_0 N_m$. For TiO_2, an average volume of a single anatase unit cell is assumed ($V_0 = 3.4 \times 10^{-23}$ cm^3, $N_m = 1$). The nonideality factor (α) describes the width of the exponential function and is typically in the range of 0.2−0.5.[13,86−88] Although N_x and V_m affect the magnitude of the fitting function, they do not affect the shape, which is dictated instead by α. The density of states function over a wide energy range fits well to an accumulation layer model proposed by Rothenberger et al. (Figure 7, green line),[54] while in the potential region of interest, which is indicated by the shaded region, $\rho(E_F)$ is exponentially distributed. The data in Figure 7 fit to eq 9 to yield $N_x = 8.6(\pm 2.5) \times 10^{18}$ cm^{-3} and $\alpha = 0.29(\pm 0.02)$, which are similar to values obtained by capacitance measurements of nanocrystalline TiO_2 films in 0.1 M hydrochloric acid.[13]

2.4. Origin of Multiexponential Decay Kinetics. Marcus−Gerischer theory predicts that with an exponentially distributed density of states, the injection rate constant (k_{inj}) should depend exponentially on the excited-state reduction potential. Shown in Figure 8 is the fast and slow decay components (k_f and k_s) for the two dye series as a function of the excited-state reduction potential, $E^{+/*}$. The linear relationship between $\ln(\tau_s^{-1})$ and $E^{+/*}$ is qualitatively consistent with Marcus−Gerischer theory and an exponential density of states distribution, $\rho_0(E)$. While Marcus−Gerischer theory can account for the slower injection component, it alone cannot explain the multiple kinetic components in the decays. Although such components often are attributed to sample heterogeneity, there are clear trends that suggest otherwise. For example, the relative contribution of the fast component (A_f) increases with the

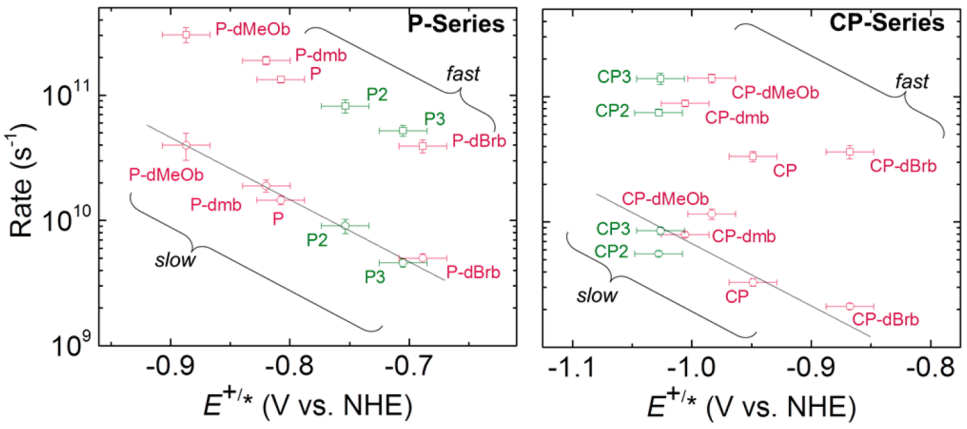

Figure 8. Plots of the fast $(\tau_f)^{-1}$ and slow $(\tau_s)^{-1}$ rates versus the dye excited-state reduction potential ($E^{+/*}$). The points in red correspond to Ru(II) dyes with a single bpyP ligand or bpyCP ligand and two ancillary ligands (**P-dRb** series or **CP-dRb** series), and green points are from the **P*x*** series or **CP*x*** dyes with two or three bpyP or bpyCP ligands. The black lines show the result of a nonlinear least-squares fit to the Marcus−Gerischer expression, eq 5, in which the coupling matrix element used to fit the **CP**-series was 4.6 times smaller than that used to fit the **P**-series.

DOI: 10.1021/jacs.5b12996
J. Am. Chem. Soc. 2016, 138, 4426−4438

electron-donating ability of the ligands, suggesting that the two kinetic components (k_f and k_s) are linked.

Scheme 1

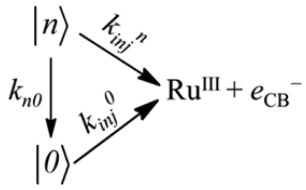

To investigate the link between k_s and k_f, we adopted the kinetic model depicted in Scheme 1. In this description, by ~1 ps the photoexcited dyes have relaxed into a distribution of states in the lower MLCT excited-state manifold. The kinetic model shown in Scheme 1 approximates this distribution of states by two levels. The lowest of the two is the thermally equilibrated (THEXI) excited state ($|0\rangle$) that decays through injection (k_{inj}^0), while the higher energy level ($|n\rangle$) decays through a combination of injection (k_{inj}^n) and relaxation to $|0\rangle$ (k_{n0}). Because the excited-state lifetimes of all the Ru(II) polypyridyl dyes are hundreds of nanoseconds, relaxation to the ground state is not included in the model. Solving the rate expression associated with this kinetic model for the time-dependent populations of $|0\rangle$ (P_t^0) and $|n\rangle$ (P_t^n) yields

$$P_t^0 = \left(P_i^0 + \frac{k_{n0}P_i^n}{k_{inj}^n + k_{n0} - k_{inj}^0}\right)e^{-k_{inj}^0 t} - \frac{k_{n0}}{k_{inj}^n + k_{n0} - k_{inj}^0} \times P_i^n e^{-(k_{inj}^n + k_{n0})t} \quad (10)$$

and

$$P_t^n = P_i^n e^{-(k_{inj}^n + k_{n0})t} \quad (11)$$

where P_i^0 and P_i^n are the populations in $|0\rangle$ and $|n\rangle$ at $t = 0$, respectively.

The normalized transient absorption signal associated with the $bpy^{\bullet-}(\pi \rightarrow \pi^*)$ absorption is the total population in the two levels, i.e.

$$\Delta\tilde{A}_t^R = \frac{(P_t^n + P_t^0)}{(P_i^n + P_i^0)} \quad (12)$$

Substituting the expressions for P_t^0 and P_t^n into eq 12, where P_t^n is written in the form $P_t^n = [k_{n0}P_i^n \exp(-(k_{inj}^n + k_{n0})t) + k_{inj}^n P_i^n \exp(-(k_{inj}^n + k_{n0})t)]/(k_{n0} + k_{inj}^n)$, and assuming that k_{inj}^0 is much less than $k_{inj}^n + k_{n0}$ yields a decay with two kinetic components, i.e.

$$\Delta\tilde{A}_t^R = \left(\frac{k_{inj}^n}{k_{inj}^n + k_{n0}} \cdot P_i^n\right)e^{-(k_{inj}^n + k_{n0})t} + \left(P_i^0 + \frac{k_{n0}}{k_{inj}^n + k_{n0}} \cdot P_i^n\right)e^{-k_{inj}^0 t} \quad (13)$$

where for simplicity we set the total initial population to unity (i.e., $P_i^0 + P_i^n = 1$). This expression enables the experimentally observed decay components and their relative amplitudes to be connected with the microscopic quantities of the kinetic model. The slower component corresponds to injection from the THEXI state (i.e., $\tau_s^{-1} \rightarrow k_{inj}^0$), while the faster decay component (τ_f^{-1}) reflects population loss from the higher energy level (i.e., $\tau_f^{-1} \rightarrow k_{inj}^n + k_{n0}$). Furthermore, because $|0\rangle$ and $|n\rangle$ are kinetically linked (i.e., population flows from $|n\rangle$ to $|0\rangle$), the relative amplitudes of the two components have a specific relationship that depends upon the magnitudes of rate constants (i.e., k_{inj}^0, k_{inj}^n, and k_{n0}) and the initial populations in the two levels, P_i^0 and P_i^n.

We demonstrate the validity of this kinetic scheme in the subsections that follow by comparing the amplitudes and decay rates predicted by eq 13 to experimental observation. Briefly, using the Marcus–Gerischer expression combined with the measured density of states, $\rho_0(E)$, and the $E^{+/*}$ values determined for each dye, we are able to calculate rate constants for injection (k_{inj}^0 and k_{inj}^n) that reproduce the trends in τ_s^{-1} and τ_f^{-1} and account for the variation among complexes. Our analysis implies an energy separation between $|0\rangle$ and $|n\rangle$ of ~0.18 eV (1400 cm^{-1}). Finally, the relative amplitudes of the two components predicted with eq 13 agree favorably with those observed experimentally across the series of dyes. This agreement implies that the fast and slow decay components are not the result of sample heterogeneity, which is often assumed, but rather a consequence of an injection process that occurs in concert with excited-state relaxation.

2.4.1. Slow Decay Component. The kinetic model depicted in Scheme 1 implies that injection from the THEXI state is represented by the slower component. Nonlinear least-squares fits of τ_s^{-1} for the two dye series to the Marcus–Gerischer expression (eq 5) are shown as solid lines in Figure 8. In this analysis, the parameters that define the shape of the density of states function (i.e., α, N_x, and E_{CB}) are determined empirically and have fixed values, while the remaining parameters H_{AB}, λ, and N_m are determined by the fit. In principle H_{AB}, λ, and N_m could all be treated as adjustable parameters; however, they are highly correlated (Figure 9) for an exponentially distributed density of states, like the one used here. As a consequence, fits in which they are treated as independent parameters result in large uncertainties in their values. An alternate strategy is to constrain the value of two (e.g., λ and N_m) and then determine the third (e.g., H_{AB}) through the fitting processes.

The values of H_{AB} were determined in this manner for a series of λ and N_m values. Because of the high degree of correlation between these parameters, the sum-of-squared errors are identical for all parameter combinations, i.e., any choice of values for λ and N_m depicted in Figure 9 yields the same fit lines shown in Figure 8. While the perfect correlation between these parameters is not surprising given the functional forms of the Marcus–Gerischer and density of states expressions, its presence makes it impossible to determine H_{AB} without making assumptions for λ and N_m. Although we do not have independent measures of either quantity, ~0.65 eV is a reasonable estimate for λ,[90,91] and it is commonly assumed that each complex is in electronic communication with only a few unit cells, i.e., $N_m \sim 1$.[52,61] Using these values for λ and N_m implies that the magnitude of H_{AB} is ~10 meV for the **P**-series and ~2–3 meV for the **CP**-series. Both values are reasonable for ruthenium-polypyridyl dyes anchored to TiO_2.[90−93] Moreover, the smaller electronic coupling that is observed for the **CP**-series is consistent with decreased electronic coupling through the saturated $-CH_2-$ spacer between the phosphonate group and bipyridine ligand, interrupting electronic communication between the dye and semiconductor acceptor levels.[94] The difference in H_{AB} values observed for the two series also suggests that the slow injection rates are not the result of physisorption or aggregation,[23] since a

DOI: 10.1021/jacs.5b12996
J. Am. Chem. Soc. 2016, 138, 4426−4438

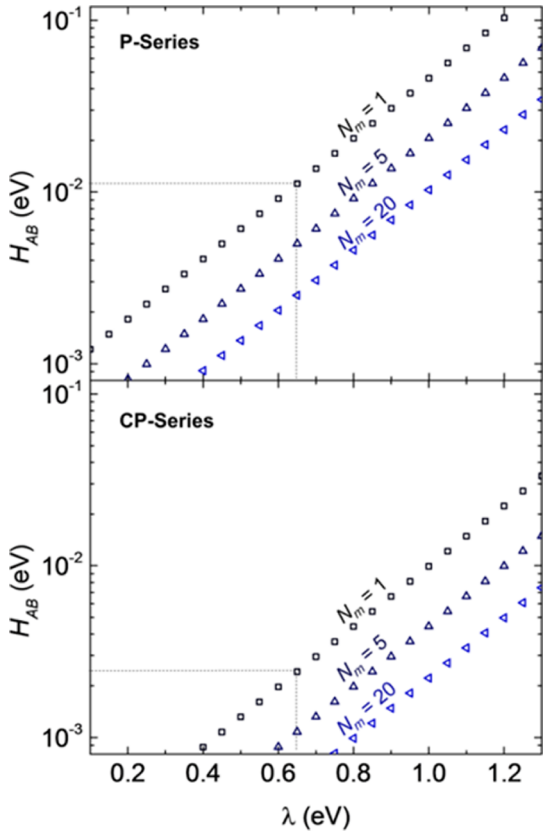

Figure 9. Correlation between reorganization energy (λ), coupling matrix element (H_{AB}), and number of interacting unit cells (N_m) that exists when fitting the Marcus–Gerischer expression (eq 5) to the observed rates and using the empirically derived density of states function.

nonspecific binding to the surface would lead to injection rates that are insensitive to the presence of the methylene group.

There are several implicit assumptions made in this analysis. First, it assumes that the dyes within a given series (**P** or **CP**) have the same value of H_{AB}, in accordance with the common notion that the electronic coupling is determined primarily by the surface linking modality of the anchoring ligand. Second, it assumes that λ is the same for all of the dyes, which is a reasonable approximation given that they all retain the $Ru(bpy)_3^{2+}$ central architecture, have oxidative electrochemistry dominated by the $Ru^{III/II}$ redox couple, and have steady-state PL spectra with similar bandwidths. Finally, and notably, it ignores interligand electron/inter-$Ru(d\pi^5)$ hole transfer (ILET) within the MLCT states. Given the discussion of the excited-state energetics above, this is likely a reasonable assumption for the **P**-series, where the lowest ^{3}MLCT state is localized on the phosphonate ligand that is bound to the surface. Previous work in our group[25] measured the time scale for ILET to be ~30 ps, in Ru(II) complexes with equal energy ligands. For modestly exergonic ligands, however, localization by ILET onto the surface bound ligand is expected to occur within a few ps after excitation. This is much faster than the slow time components for the **P**-series (e.g., 53 ps in **P-dmb**), suggesting that ILET is not the origin of the slower injection component for this series of dyes.

The ILET process may play a role, however, in the **P-dRbr** complex and the complexes in the **CP**-series, where the ligands appear to be nearly isoenergetic, which could account for the increased scatter observed in the injection rates for the **CP**-series. In the case of the **CP-dBrb** complex, the ancillary ligand is likely lowest in energy, implying that injection is either preceded by ILET or occurs directly from the remote ligand.

2.4.2. Fast Decay Component. The fast component is characterized by decay constant (τ_f^{-1}) and an amplitude (A_f), which in the context of this kinetic model are determined by the rate constants for injection (k_{inj}^n) and $|n\rangle \rightarrow |0\rangle$ relaxation (k_{n0}) as well as the initial population in $|n\rangle$ (P_i^n), i.e.

$$(\tau_f)^{-1} = k_{inj}^n + k_{n0} \tag{14}$$

and

$$A_f = \frac{k_{inj}^n}{k_{inj}^n + k_{n0}} \cdot P_i^n \tag{15}$$

Rearranging eq 15 and using $k_{inj}^n = k_{n0} - (\tau_f)^{-1}$ reveals a linear relationship between the experimentally observed quantities (A_f and τ_f) and two of the parameters in the kinetic model (k_{n0} and P_i^n), i.e.

$$A_f = P_i^n - k_{n0} P_i^n \tau_f \tag{16}$$

where the y-intercept and slope are P_i^n and $-k_{n0}P_i^n$, respectively. Shown in Figure 10 are the amplitudes as a function of the

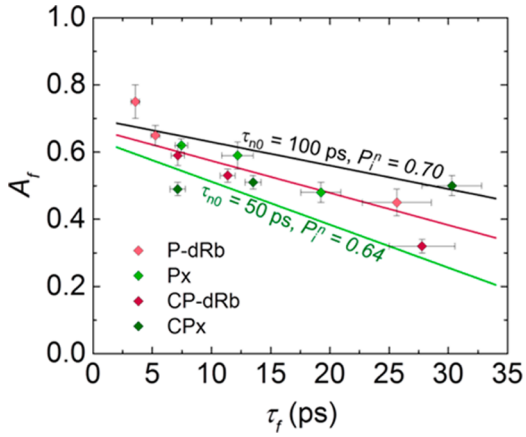

Figure 10. Comparison of amplitudes and fast time constants resulting from fits to picosecond electron injection for the 12 Ru(II) polypyridyl dyes studied here. The lines are fits to the data using eq 15. The best fit (red line) obtained by least-squares was with a rate constant ($k_{n0} = \tau_{n0}^{-1}$) of ~ $(70\ ps)^{-1}$ and initial population (P_i^n) of 0.67.

lifetime for the 12 dyes studied. The clear correlation between amplitude and time constant of the fast component across all 12 dyes supports the validity of the kinetic model depicted in Scheme 1. A linear fit of the experimental amplitudes to eq 16 yields values for P_i^n and k_{n0} that are $(70\ ps)^{-1}$ and 0.67, respectively (Figure 10, red line). The green and black lines that bracket the data in Figure 10 illustrate the sensitivity of eq 16 to the kinetic model parameters, suggesting that P_i^n is between 0.7 and 0.64 and k_{n0} is between $(50\ ps)^{-1}$ and $(100\ ps)^{-1}$.

The energy difference between the $|0\rangle$ and $|n\rangle$ (ΔG_{n0}) is obtained by applying the Marcus–Gerischer expression to injection from the higher energy state (k_{inj}^n), which is achieved by adding ΔG_{n0} to the driving force expression for $|0\rangle$, i.e.

$$\Delta G\varepsilon_n = \Delta G(E^{+/*}) + \Delta G_{n0} \tag{17}$$

while keeping all of the other parameters (i.e., H_{AB}, λ, N_m, and $\rho_0(E)$) the same as for the slow component. Combined with the

DOI: 10.1021/jacs.5b12996
J. Am. Chem. Soc. 2016, 138, 4426–4438

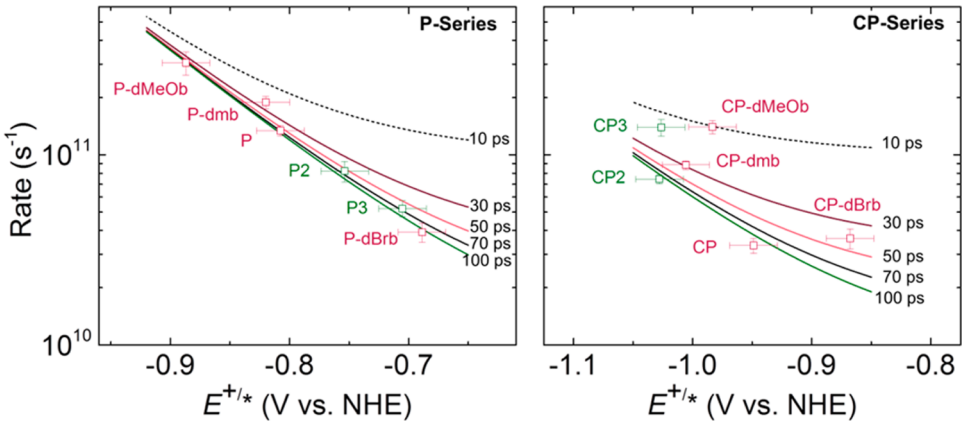

Figure 11. Plot of the fast observed rate constant (τ_f^{-1}) showing fits to Marcus−Gerischer theory using different interstate relaxation times (τ_{n0}). In all sets of fits, a difference of −0.18 eV in injecting state free energy (ΔG_{n0}) between $|n\rangle$ and $|0\rangle$ populations is used.

preceding analysis of the amplitudes, the experimental observables describing the fast decay component (τ_f^{-1} and A_f) are then determined by three microscopic parameters (ΔG_{n0}, k_{n0}, and P_i^n).

The fast rate constants (τ_f^{-1}) for the **P**-series are fit to eq 5 with k_{n0} set to $(70\ \text{ps})^{-1}$, leaving ΔG_{n0} as the only adjustable parameter (Figure 11). The best fit curve is obtained with a ΔG_{n0} of −0.18 eV (1400 cm^{-1}). Also shown in the figure are a series of curves corresponding to different values of the relaxation rate ranging from $(10\ \text{ps})^{-1}$ to $(100\ \text{ps})^{-1}$. While relaxation rates between $(50\ \text{ps})^{-1}$ and $(100\ \text{ps})^{-1}$ all provide reasonable agreement with the experimental data, comparison with the other curves suggests that an upper limit to the rate would be ∼ $(30\ \text{ps})^{-1}$.

While this analysis indicates that injection is occurring from two different excited states, it does not specify the identity of the higher level, of which there are several possibilities. The free energy difference of 1400 cm^{-1}, which is observed if H_{AB} in $|0\rangle$ and $|n\rangle$ are equal, is remarkably similar to the mode spacing ($h\omega$) found in the Franck−Condon analysis of the PL spectra (Table S2), suggesting that $|n\rangle$ could be a vibrationally hot state in the same ^{3}MLCT manifold as $|0\rangle$. While the ∼70 ps relaxation time that is inferred from the kinetic model is comparable to vibrational cooling times observed in several dye systems,[95] it is longer than the 7−20 ps that has been reported for Ru(II) complexes in solution.[25,32,74,96] One possible explanation for this discrepancy is that the longer relaxation time could reflect the final stages of an internal conversion process in the ^{3}MLCT state that is initially fast but slows as the internal energy decreases,[97] perhaps as a result of the smaller temperature difference with the solvent that occurs as the internal energy in the molecule is deposited into its surroundings. Another possibility is that this slower relaxation could be a consequence of reduced solvent access when the complexes are bound to the surface. Transient spectra for the **P** dye in solution and on ZrO_2, where injection is thermodynamically unfavorable, show spectral evolution with a ∼ 100 ps time constant that is unique to the surface (Figure S9), supporting the presence of a relaxation process on the excited state that was inferred from the kinetic model.

Other possibilities emerge if the two states do not have the same electronic coupling with the surface.[97] For example, if H_{AB} for $|n\rangle$ is 1.25 times greater than that of $|0\rangle$ in the fit (i.e., 11 vs 14 meV), the best fit is obtained with ΔG_{n0} equal to −0.12 eV (1000 cm^{-1}), and if H_{AB} is doubled from 11 to 22 meV when λ = 0.65 eV, the best fit yields ΔG_{n0} = −0.06 eV (500 cm^{-1}). These free energy differences are consistent with a higher energy ^{3}MLCT state (so-called fourth ^{3}MLCT state), which is known to influence the PL lifetimes.[74,98−105] In this scenario k_{n0} would reflect the relaxation to the low-energy ^{3}MLCT state. Regardless of the physical origin associated with this relaxation process, this simple kinetic model depicted in Scheme 1 accounts for the observed multiexponential injection behavior.

The model of competitive injection and relaxation holds if we extend it to include the ultrafast injection component observed shortly following excitation. The optically prepared state samples TiO_2 acceptor levels ∼1 eV higher than the thermally equilibrated state, corresponding to an approximately 1000-fold increase in the density of TiO_2 acceptor levels. Because the probability of injection is a product of coupling matrix element and the density of available acceptor levels, our model predicts an injection rate of approximately $(69\ \text{fs})^{-1}$ for the dye **P**, without changing the coupling or reorganization energy. This is consistent with an earlier report by Giokas et al.[32] in which the **P*x***- and **CP*x***-series was observed to have injection components in the tens to hundreds of femtoseconds, respectively. While we do not discount the possibility that coupling varies with energy, it does not appear to be the main driver for the multiple time scales observed in the injection kinetics.

3. CONCLUSION

The electron injection kinetics from 12 structurally related photoexcited Ru(II) polypyridyl dyes into subconduction band levels of titanium dioxide are described. Using a combination of femtosecond transient absorption spectroscopy, careful sample preparation, and detailed thermodynamic and kinetic analysis of the family of 12 Ru(II) polypyridyl dyes in which the excited-state reduction potentials have been systematically tuned, we show that injection on slower time scales is indeed from surface attached dyes and that the kinetic heterogeneity arises as a result of competition between excited-state relaxation and injection from within the same manifold of dye excited states. Thusly, we provide a framework for reproducing injection rates on slower time scales for a broad range of dyes using a set of experimentally derived parameters.

■ ASSOCIATED CONTENT

Supporting Information

The Supporting Information is available free of charge on the ACS Publications website at DOI: 10.1021/jacs.5b12996.

DOI: 10.1021/jacs.5b12996
J. Am. Chem. Soc. 2016, 138, 4426−4438

The summarized experimental methods are presented in the Supporting Information. Also presented are a comparison of the transient absorption spectra for **CP-dmb** on ZrO_2 and TiO_2, the results of emission spectral fitting, images of all the molecular orbitals calculated by DFT, tables of electrochemical data, results of spectroelectrochemical measurements of a nano-TiO_2, a comparison of fitting decays to a biexponential function and stretched exponential (Kohlrausch–Williams–Watts), and a comparison of the picosecond spectral evolution in solution and on ZrO_2. Finally, the kinetic model in eq 13 is derived(PDF)

AUTHOR INFORMATION

Corresponding Authors

*john_papanikolas@unc.edu
*dfzigler@email.unc.edu

Notes

The authors declare no competing financial interest.

ACKNOWLEDGMENTS

Funding for this work was provided solely through the UNC EFRC: Center for Solar Fuels, an Energy Frontier Research Center funded by the U.S. Department of Energy, Office of Science, Office of Basic Energy Sciences under award no. DE-SC0001011. D.L.A. acknowledges support from an individual fellowship from the Department of Energy Office of Science Graduate Fellowship Program (DOE SCGF), made possible in part by the American Recovery and Reinvestment Act of 2009, administered by ORISE-ORAU under contract no. DE-AC05-06OR23100. We thank Prof. Andrew M. Moran, Robert J. Brown, Paul G. Giokas, and Thomas P. Cheshire for helpful discussion.

REFERENCES

(1) O'Regan, B.; Grätzel, M. *Nature* **1991**, *353*, 737.
(2) Hagfeldt, A.; Boschloo, G.; Sun, L.; Kloo, L.; Pettersson, H. *Chem. Rev.* **2010**, *110*, 6595.
(3) Meyer, T. J. *Acc. Chem. Res.* **1989**, *22*, 163.
(4) Concepcion, J. J.; House, R. L.; Papanikolas, J. M.; Meyer, T. J. *Proc. Natl. Acad. Sci. U. S. A.* **2012**, *109*, 15560.
(5) Ardo, S.; Meyer, G. J. *Chem. Soc. Rev.* **2009**, *38*, 115.
(6) Grätzel, M. *Acc. Chem. Res.* **2009**, *42*, 1788.
(7) Mishra, A.; Fischer, M. K. R.; Bäuerle, P. *Angew. Chem., Int. Ed.* **2009**, *48*, 2474.
(8) Asbury, J. B.; Hao, E.; Wang, Y.; Ghosh, H. N.; Lian, T. *J. Phys. Chem. B* **2001**, *105*, 4545.
(9) Haque, S. A.; Tachibana, Y.; Willis, R. L.; Moser, J. E.; Grätzel, M.; Klug, D. R.; Durrant, J. R. *J. Phys. Chem. B* **2000**, *104*, 538.
(10) Tachibana, Y.; Haque, S. A.; Mercer, I. P.; Moser, J. E.; Klug, D. R.; Durrant, J. R. *J. Phys. Chem. B* **2001**, *105*, 7424.
(11) Lyon, L. A.; Hupp, J. T. *J. Phys. Chem. B* **1999**, *103*, 4623.
(12) O'Regan, B.; Xiaoe, L.; Ghaddar, T. *Energy Environ. Sci.* **2012**, *5*, 7203.
(13) Bertoluzzi, L.; Herraiz-Cardona, I.; Gottesman, R.; Zaban, A.; Bisquert, J. *J. Phys. Chem. Lett.* **2014**, *5*, 689.
(14) Tachibana, Y.; Moser, J. E.; Grätzel, M.; Klug, D. R.; Durrant, J. R. *J. Phys. Chem.* **1996**, *100*, 20056.
(15) Hannappel, T.; Burfeindt, B.; Storck, W.; Willig, F. *J. Phys. Chem. B* **1997**, *101*, 6799.
(16) Benkö, G.; Kallioinen, J.; Korppi-Tommola, J.; Yartsev, A. P.; Sundström, V. *J. Am. Chem. Soc.* **2002**, *124*, 489.
(17) Kuciauskas, D.; Monat, J. E.; Villahermosa, R.; Gray, H. B.; Lewis, N. S.; McCusker, J. K. *J. Phys. Chem. B* **2002**, *106*, 9347.
(18) Miller, S. A.; West, B. A.; Curtis, A. C.; Papanikolas, J. M.; Moran, A. M. *J. Chem. Phys.* **2011**, *135*, 081101.
(19) Ramakrishna, S.; Willig, F.; May, V.; Knorr, A. *J. Phys. Chem. B* **2003**, *107*, 607.
(20) Ernstorfer, R.; Gundlach, L.; Felber, S.; Storck, W.; Eichberger, R.; Willig, F. *J. Phys. Chem. B* **2006**, *110*, 25383.
(21) Ramakrishna, S.; Willig, F.; May, V. *Chem. Phys. Lett.* **2002**, *351*, 242.
(22) Redfern, P. C.; Zapol, P.; Curtiss, L. A.; Rajh, T.; Thurnauer, M. C. *J. Phys. Chem. B* **2003**, *107*, 11419.
(23) Wenger, B.; Grätzel, M.; Moser, J.-E. *J. Am. Chem. Soc.* **2005**, *127*, 12150.
(24) Shaw, G. B.; Brown, C. L.; Papanikolas, J. M. *J. Phys. Chem. A* **2002**, *106*, 1483.
(25) Shaw, G. B.; Styers-Barnett, D. J.; Gannon, E. Z.; Granger, J. C.; Papanikolas, J. M. *J. Phys. Chem. A* **2004**, *108*, 4998.
(26) Damrauer, N. H.; McCusker, J. K. *J. Phys. Chem. A* **1999**, *103*, 8440.
(27) Hewitt, J. T.; Vallett, P. J.; Damrauer, N. H. *J. Phys. Chem. A* **2012**, *116*, 11536.
(28) Browne, W. R.; Passaniti, P.; Gandolfi, M. T.; Ballardini, R.; Henry, W.; Guckian, A.; O'Boyle, N.; McGarvey, J. J.; Vos, J. G. *Inorg. Chim. Acta* **2007**, *360*, 1183.
(29) Henry, W.; Coates, C. G.; Brady, C.; Ronayne, K. L.; Matousek, P.; Towrie, M.; Botchway, S. W.; Parker, A. W.; Vos, J. G.; Browne, W. R.; McGarvey, J. J. *J. Phys. Chem. A* **2008**, *112*, 4537.
(30) Wallin, S.; Davidsson, J.; Modin, J.; Hammarström, L. *J. Phys. Chem. A* **2005**, *109*, 4697.
(31) Kallioinen, J.; Benkö, G.; Sundström, V.; Korppi-Tommola, J. E. I.; Yartsev, A. P. *J. Phys. Chem. B* **2002**, *106*, 4396.
(32) Giokas, P. G.; Miller, S. A.; Hanson, K.; Norris, M. R.; Glasson, C. R. K.; Concepcion, J. J.; Bettis, S. E.; Meyer, T. J.; Moran, A. M. *J. Phys. Chem. C* **2013**, *117*, 812.
(33) Asbury, J. B.; Anderson, N. A.; Hao, E.; Ai, X.; Lian, T. *J. Phys. Chem. B* **2003**, *107*, 7376.
(34) Bettis, S. E.; Hanson, K.; Wang, L.; Gish, M. K.; Concepcion, J. J.; Fang, Z.; Meyer, T. J.; Papanikolas, J. M. *J. Phys. Chem. A* **2014**, *118*, 10301.
(35) Bettis, S. E.; Ryan, D. M.; Gish, M. K.; Alibabaei, L.; Meyer, T. J.; Waters, M. L.; Papanikolas, J. M. *J. Phys. Chem. C* **2014**, *118*, 6029.
(36) Juozapavicius, M.; Kaucikas, M.; Dimitrov, S. D.; Barnes, P. R. F.; van Thor, J. J.; O'Regan, B. C. *J. Phys. Chem. C* **2013**, *117*, 25317.
(37) Persson, P.; Lundqvist, M. J.; Ernstorfer, R.; Goddard, W. A.; Willig, F. *J. Chem. Theory Comput.* **2006**, *2*, 441.
(38) Gundlach, L.; Willig, F. *ChemPhysChem* **2012**, *13*, 2877.
(39) Gundlach, L.; Burfeindt, B.; Mahrt, J.; Willig, F. *Chem. Phys. Lett.* **2012**, *545*, 35.
(40) Prezhdo, O. V.; Duncan, W. R.; Prezhdo, V. V. *Prog. Surf. Sci.* **2009**, *84*, 30.
(41) Akimov, A. V.; Asahi, R.; Jinnouchi, R.; Prezhdo, O. V. *J. Am. Chem. Soc.* **2015**, *137*, 11517.
(42) Bauer, C.; Teuscher, J.; Pelet, S.; Wenger, B.; Bonhote, P.; Nazeeruddin, M. K.; Zakeeruddin, S. M.; Comte, P.; Grätzel, M.; Moser, J. E. *Curr. Sci.* **2010**, *99*, 343.
(43) Benkö, G.; Kallioinen, J.; Myllyperkiö, P.; Trif, F.; Korppi-Tommola, J. E. I.; Yartsev, A. P.; Sundström, V. *J. Phys. Chem. B* **2004**, *108*, 2862.
(44) Liu, F.; Meyer, G. J. *Inorg. Chem.* **2005**, *44*, 9305.
(45) Li, C.; Koenigsmann, C.; Ding, W.; Rudshteyn, B.; Yang, K. R.; Regan, K. P.; Konezny, S. J.; Batista, V. S.; Brudvig, G. W.; Schmuttenmaer, C. A.; Kim, J.-H. *J. Am. Chem. Soc.* **2015**, *137*, 1520.
(46) Christianson, J. R.; Schmidt, J. R. *Phys. Chem. Chem. Phys.* **2015**, *17*, 3731.
(47) Laaser, J. E.; Christianson, J. R.; Oudenhoven, T. A.; Joo, Y.; Gopalan, P.; Schmidt, J. R.; Zanni, M. T. *J. Phys. Chem. C* **2014**, *118*, 5854.
(48) Teuscher, J.; Décoppet, J.-D.; Punzi, A.; Zakeeruddin, S. M.; Moser, J.-E.; Grätzel, M. *J. Phys. Chem. Lett.* **2012**, *3*, 3786.

DOI: 10.1021/jacs.5b12996
J. Am. Chem. Soc. 2016, 138, 4426–4438

(49) Paoprasert, P.; Laaser, J. E.; Xiong, W.; Franking, R. A.; Hamers, R. J.; Zanni, M. T.; Schmidt, J. R.; Gopalan, P. *J. Phys. Chem. C* **2010**, *114*, 9898.
(50) Oudenhoven, T. A.; Joo, Y.; Laaser, J. E.; Gopalan, P.; Zanni, M. T. *J. Chem. Phys.* **2015**, *142*, 212449.
(51) Anderson, N. A.; Ai, X.; Chen, D.; Mohler, D. L.; Lian, T. *J. Phys. Chem. B* **2003**, *107*, 14231.
(52) De Angelis, F.; Fantacci, S.; Selloni, A.; Grätzel, M. *Nano Lett.* **2007**, *7*, 3189.
(53) Kallioinen, J.; Benkö, G.; Myllyperkiö, P.; Khriachtchev, L.; Skårman, B.; Wallenberg, R.; Tuomikoski, M.; Korppi-Tommola, J.; Sundström, V.; Yartsev, A. P. *J. Phys. Chem. B* **2004**, *108*, 6365.
(54) Rothenberger, G.; Fitzmaurice, D.; Grätzel, M. *J. Phys. Chem.* **1992**, *96*, 5983.
(55) She, C.; Guo, J.; Lian, T. *J. Phys. Chem. B* **2007**, *111*, 6903.
(56) Juris, A.; Balzani, V.; Barigletti, F.; Campagna, S.; Belser, P.; Von Zelewsky, A. *Coord. Chem. Rev.* **1988**, *84*, 85.
(57) Ai, X.; Guo, J.; Anderson, N. A.; Lian, T. *J. Phys. Chem. B* **2004**, *108*, 12795.
(58) Anderson, N. A.; Ai, X.; Lian, T. *J. Phys. Chem. B* **2003**, *107*, 14414.
(59) Guo, J.; Stockwell, D.; Ai, X.; She, C.; Anderson, N. A.; Lian, T. *J. Phys. Chem. B* **2006**, *110*, 5238.
(60) Huang, J.; Stockwell, D.; Boulesbaa, A.; Guo, J.; Lian, T. *J. Phys. Chem. C* **2008**, *112*, 5203.
(61) She, C.; Anderson, N. A.; Guo, J.; Liu, F.; Goh, W.-H.; Chen, D.-T.; Mohler, D. L.; Tian, Z.-Q.; Hupp, J. T.; Lian, T. *J. Phys. Chem. B* **2005**, *109*, 19345.
(62) Yoshimura, A.; Hoffman, M. Z.; Sun, H. *J. Photochem. Photobiol., A* **1993**, *70*, 29.
(63) Wang, L.; Ashford, D. L.; Thompson, D. W.; Meyer, T. J.; Papanikolas, J. M. *J. Phys. Chem. C* **2013**, *117*, 24250.
(64) Knauf, R. R.; Brennaman, M. K.; Alibabaei, L.; Norris, M. R.; Dempsey, J. L. *J. Phys. Chem. C* **2013**, *117*, 25259.
(65) Li, L.; Giokas, P. G.; Kanai, Y.; Moran, A. M. *J. Chem. Phys.* **2014**, *140*, 234109.
(66) Miller, S. A.; Moran, A. M. *J. Phys. Chem. A* **2010**, *114*, 2117.
(67) Molesky, B. P.; Moran, A. M. *J. Phys. Chem. A* **2013**, *117*, 13954.
(68) Although we do not use τ_{uf} in fitting our data, the process giving rise to this time constant is centrally important to understanding the partition of vibrationally hot and thermally equilibrated excited states discussed within our kinetic model.
(69) Marcus, R. A. *Annu. Rev. Phys. Chem.* **1964**, *15*, 155.
(70) Hush, N. S. *Trans. Faraday Soc.* **1961**, *57*, 557.
(71) Gerischer, H. *Pure Appl. Chem.* **1980**, *52*, 2649.
(72) The negative sign in front of the integral expression accounts for the convention that higher energy states appear at more negative electrochemical potentials, i.e., $E_{\emptyset} > E_{vac}$.
(73) Schoonover, J. R.; Dattelbaum, D. M.; Malko, A.; Klimov, V. I.; Meyer, T. J.; Styrers-Barnett, D. J.; Gannon, E. Z.; Granger, J. C.; Aldridge, W. S., III; Papanikolas, J. M. *J. Phys. Chem. A* **2005**, *109*, 2472.
(74) Hager, G. D.; Watts, R. J.; Crosby, G. A. *J. Am. Chem. Soc.* **1975**, *97*, 7037.
(75) Marcus, R. A.; Sutin, N. *Comments Inorg. Chem.* **1986**, *5*, 119.
(76) Hupp, J. T.; Neyhart, G. A.; Meyer, T. J.; Kober, E. M. *J. Phys. Chem.* **1992**, *96*, 10820.
(77) Claude, J.-P. *Photophysics of polypyridyl complexes of Ru(II), Os(II), and Re(I)*, The University of North Carolina at Chapel Hill, 1995.
(78) Thompson, D. G.; Schoonover, J. R.; Timpson, C. J.; Meyer, T. J. *J. Phys. Chem. A* **2003**, *107*, 10250.
(79) Ito, A.; Stewart, D. J.; Knight, T. E.; Fang, Z.; Brennaman, M. K.; Meyer, T. J. *J. Phys. Chem. B* **2013**, *117*, 3428.
(80) Lever, A. B. P. *Inorg. Chem.* **1990**, *29*, 1271.
(81) Bailes, M.; Cameron, P. J.; Lobato, K.; Peter, L. M. *J. Phys. Chem. B* **2005**, *109*, 15429.
(82) Nunzi, F.; Storchi, L.; Manca, M.; Giannuzzi, R.; Gigli, G.; De Angelis, F. *ACS Appl. Mater. Interfaces* **2014**, *6*, 2471.
(83) Boschloo, G.; Fitzmaurice, D. *J. Phys. Chem. B* **1999**, *103*, 7860.
(84) Fitzmaurice, D. *Sol. Energy Mater. Sol. Cells* **1994**, *32*, 289.
(85) Bisquert, J.; Fabregat-Santiago, F.; Mora-Seró, I.; Garcia-Belmonte, G.; Barea, E. M.; Palomares, E. *Inorg. Chim. Acta* **2008**, *361*, 684.
(86) Abayev, I.; Zaban, A.; Kytin, V. G.; Danilin, A. A.; Garcia-Belmonte, G.; Bisquert, J. *J. Solid State Electrochem.* **2007**, *11*, 647.
(87) Bisquert, J. *Phys. Rev. B: Condens. Matter Mater. Phys.* **2008**, *77*, 235203.
(88) Fabregat-Santiago, F.; Garcia-Belmonte, G.; Mora-Sero, I.; Bisquert, J. *Phys. Chem. Chem. Phys.* **2011**, *13*, 9083.
(89) Boschloo, G.; Fitzmaurice, D. *J. Phys. Chem. B* **1999**, *103*, 2228.
(90) Brown, G. M.; Sutin, N. *J. Am. Chem. Soc.* **1979**, *101*, 883.
(91) Farnum, B. H.; Morseth, Z. A.; Brennaman, M. K.; Papanikolas, J. M.; Meyer, T. J. *J. Am. Chem. Soc.* **2014**, *136*, 15869.
(92) Winkler, J. R.; Gray, H. B. *Chem. Rev.* **1992**, *92*, 369.
(93) Farnum, B. H.; Morseth, Z. A.; Brennaman, M. K.; Papanikolas, J. M.; Meyer, T. J. *J. Phys. Chem. B* **2015**, *119*, 7698.
(94) Gray, H. B.; Winkler, J. R. *Proc. Natl. Acad. Sci. U. S. A.* **2005**, *102*, 3534.
(95) Elsaesser, T.; Kaiser, W. *Annu. Rev. Phys. Chem.* **1991**, *42*, 83.
(96) Canton, S. E.; Kjær, K. S.; Vankó, G.; van Driel, T. B.; Adachi, S.-i.; Bordage, A.; Bressler, C.; Chabera, P.; Christensen, M.; Dohn, A. O.; Galler, A.; Gawelda, W.; Gosztola, D.; Haldrup, K.; Harlang, T.; Liu, Y.; Møller, K. B.; Németh, Z.; Nozawa, S.; Pápai, M.; Sato, T.; Sato, T.; Suarez-Alcantara, K.; Togashi, T.; Tono, K.; Uhling, J.; Vithanage, D. A.; Wärnmark, K.; Yabashi, M.; Zhang, J.; Sundström, V.; Nielsen, M. M. *Nat. Commun.* **2015**, *6*, 6359.
(97) Fleming, G. R. *Chemical Applications in Ultrafast Spectroscopy*; Oxford University Press: New York, 1986; Vol. *13*.
(98) Yersin, H.; Humbs, W.; Strasser, J. *Coord. Chem. Rev.* **1997**, *159*, 325.
(99) Allsopp, S. R.; Cox, A.; Jenkins, S. H.; Kemp, T. J.; Tunstall, S. M. *Chem. Phys. Lett.* **1976**, *43*, 135.
(100) Yersin, H.; Gallhuber, E. *J. Am. Chem. Soc.* **1984**, *106*, 6582.
(101) Crosby, G. A.; Elfring, W. H. J. *J. Phys. Chem.* **1976**, *80*, 2206.
(102) Hager, G. D.; Crosby, G. A. *J. Am. Chem. Soc.* **1975**, *97*, 7031.
(103) Allsopp, S. R.; Cox, A.; Kemp, T. J.; Reed, W. J. *J. Chem. Soc., Faraday Trans. 1* **1978**, *74*, 1275.
(104) Harriman, A.; Izzet, G. *Phys. Chem. Chem. Phys.* **2007**, *9*, 944.
(105) O'Donnell, R. M.; Johansson, P. G.; Abrahamsson, M.; Meyer, G. J. *Inorg. Chem.* **2013**, *52*, 6839.

DOI: 10.1021/jacs.5b12996
J. Am. Chem. Soc. 2016, 138, 4426−4438